

## Article

# Drug Release Kinetics of DOX-Loaded Graphene-Based Nanocarriers for Ovarian and Breast Cancer Therapeutics

Katherine Taylor <sup>1</sup>, Tanveer A. Tabish <sup>2,3</sup>  and Roger J. Narayan <sup>4,\*</sup> 

<sup>1</sup> Department of Mechanical Engineering, University College London, London WC1E 7JE, UK; Katherine.taylor.20@ucl.ac.uk

<sup>2</sup> UCL Cancer Institute, University College London, London WC1E 6DD, UK; T.tabish@imperial.ac.uk

<sup>3</sup> Department of Materials and London Centre for Nanotechnology, Imperial College London, London SW7 2AZ, UK

<sup>4</sup> Joint Department of Biomedical Engineering, University of North Carolina and North Carolina State University, Raleigh, NC 27695-7907, USA

\* Correspondence: Roger\_narayan@unc.edu

**Abstract:** Cancer remains one of the leading causes of death worldwide despite extensive efforts at developing curative treatments. Chemotherapy, one of the most common forms of treatment, lacks specificity and can induce collateral damages to healthy surrounding tissues/cells and elicit off-target toxic side effects. The carbon-based nanomaterial graphene, can load aromatic drugs with high efficiency, has good biocompatibility, and can be easily functionalised with targeting ligands, antibodies, and biomolecules to increase the accuracy of targeting specific areas; graphene has therefore been explored as a nanocarrier for classical chemotherapy drugs. In this work, seventeen publications that report the release of doxorubicin (DOX) from 2D graphene-based nanohybrids (graphene oxide and reduced graphene oxide) for the treatment of breast and ovarian cancers have been identified based on a range of inclusion and exclusion criteria. To aid in the clinical translation of proof-of-concept studies, this work identifies the pre-clinical experimental protocols and analyses the release kinetics of these publications. Fifteen of the papers utilised a change in pH as the stimulus for drug release, and two utilised either near infrared (NIR) or ultrasound as the stimulus. The extracted drug release data from these publications were fit to four known kinetic models. It was found that the majority of these data best fit the Weibull kinetic model. The agreement between the kinetic data in previously published literature provides a predictable estimation of DOX release from graphene-based nanocarriers. This study demonstrates the potential conjugation of graphene and DOX in drug delivery applications, and this knowledge can help improve to the design and formulation of future graphene-based nanocarriers. In addition, the use of further experimental testing and the standardisation of experimental protocols will be beneficial for future work. The incorporation of computational modelling prior to pre-clinical testing will also aid in the development of controlled and sustained DOX release systems that offer efficient and efficacious results.

**Keywords:** graphene-based nanocarriers; doxorubicin; ovarian cancer; breast cancer; drug release kinetics; kinetic models; targeted delivery



**Citation:** Taylor, K.; Tabish, T.A.; Narayan, R.J. Drug Release Kinetics of DOX-Loaded Graphene-Based Nanocarriers for Ovarian and Breast Cancer Therapeutics. *Appl. Sci.* **2021**, *11*, 11151. <https://doi.org/10.3390/app112311151>

Academic Editor: Agnese Magnani

Received: 5 October 2021

Accepted: 22 November 2021

Published: 24 November 2021

**Publisher's Note:** MDPI stays neutral with regard to jurisdictional claims in published maps and institutional affiliations.



**Copyright:** © 2021 by the authors. Licensee MDPI, Basel, Switzerland. This article is an open access article distributed under the terms and conditions of the Creative Commons Attribution (CC BY) license (<https://creativecommons.org/licenses/by/4.0/>).

## 1. Introduction

Cancer is the second leading cause of death worldwide, and was associated with nearly 10 million deaths globally in 2020 [1,2]. Specifically, ovarian and breast cancer caused 207,252 and 684,996 global deaths, respectively, in 2020 [2]. The complexity of cancer, however, has meant that despite extensive research efforts, the treatments and therapies available are focused on extending survival; the only curative treatment is to surgically remove tumours in early-stage cancers [3]. Current available therapies and treatments that patients can receive include chemotherapy, surgery, radiotherapy, immunotherapy,

photodynamic therapy (PDT), and photothermal therapy (PTT). Treatment is highly dependent on the type of cancer and the progression of the disease. One of the most common treatments is chemotherapy, which utilises toxic agents to kill cancerous cells but often consequently induces collateral damages to healthy tissues due to the off-target toxic side effects that are associated with chemotherapy [4]. To eliminate the off-target toxic side effects of chemotherapeutic agents, cancer therapy requires the use of targeted drug delivery platforms. Nanomaterials offer the opportunity to accurately target the site of interest while reducing the dosage required to elicit an effect.

Nanoscience is the study and manipulation of materials on a scale of 1–100 nm, which brings together multiple disciplines, including physics, engineering, materials science, biology, and medicine [5]. In the last century nanotechnology has been implemented into a range of different fields, such as food and agriculture, electronics, energy, and cosmetics. The most significant advances, however, have been in biomedicine and healthcare [5,6]. Nanomedicine is the application of nanotechnology in medicine, with the goal of improving healthcare and current treatments and controlling and preventing diseases through diagnostics, imaging, and therapeutics [7,8]. Nanomaterials themselves can be defined as manufactured materials with one or more external dimensions in the nanoscale range of 1–100 nm [9,10].

Nanomaterials offer unique physical characteristics that are often very different from their larger counterparts due to their small size and large surface area to volume ratio. Furthermore, nanomaterials can be engineered to alter their optical, electrical, mechanical, and magnetic properties, as well as their size, shape, and chemical composite to make them most suited for their intended application [10,11]. These properties offer unique advantages and have been utilised for therapeutics, diagnostics, and imaging within the healthcare field. In addition, many biological mechanisms within the body take place on a nanoscale, meaning that nanomaterials can move freely and have a great opportunity to cross natural barriers, be taken up by cells, interact with biomolecules, and bind receptors [7].

The favourable characteristics of nanoparticles (NPs) have seen the rapid development of nanoparticle-mediated drug delivery systems for use in neurodegenerative, infectious, and autoimmune diseases, as well as in cancer applications; there are currently a host of NPs that have been approved for clinical use by the Food and Drug Administration (FDA). A more detailed account of the FDA-approved therapeutic NPs and those currently in clinical and pre-clinical trials is beyond the scope of this research paper. Readers can be directed to the following papers for more information [12–15]. Principally, targeted nano-delivery systems are being extensively developed for use in cancer treatments; more than 20% of the therapeutic NPs approved and in pre-clinical or clinical trials have been developed for anti-cancer applications [12].

Among nanomaterials, graphene has recently emerged as a promising agent for use in diagnostic and therapeutic applications. Graphene is a 2D planar carbon structure composed of a one atom-thick sheet of  $sp^2$  hybridised carbon atoms arranged in a hexagonal crystal lattice. Graphene is the basis of many other carbon structures, such as 3D graphite which is formed through the stacking of graphene, the isolation of single-layer graphite in the form of 2D graphene, 1D nanotubes formed by rolling the graphene, and 0D fullerenes formed by wrapping the graphene sheets into spherical structures [4,16,17]. Graphene's structure offers unique mechanical, optical, thermal, and electronic properties that are very attractive for use in biomedical applications. Graphene has an extremely large surface area that is calculated at  $2630 \text{ m}^2 \text{ g}^{-1}$ , a strong Young's modulus of 1100 GPa, and a high thermal conductivity of  $5000 \text{ W m}^{-1} \text{ K}^{-1}$  [18].

Graphene is found in the form of graphene oxide (GO), reduced GO (rGO), graphene nanoribbons, nanoplatelets, quantum dots (QDs), aerogels, and foam. The structure of GO (Figure 1) can most commonly be described using the Lerf-Kilnowski model which describes GO as a planar  $sp^2$  hybridised hexagonal lattice decorated with  $sp^3$  alcohol or epoxide bonds, with carboxylic acid groups populating the edges [17]. GO prepared by the Hummer's method retains many of the favourable characteristics of graphene, but

the oxygenated functional groups make the material hydrophilic, thereby increasing its solubility and providing additional points of binding for molecules [17]. Through chemical, electrochemical, or thermal reduction, rGO can also be synthesised, which restores the electrical conductivity of GO [18].

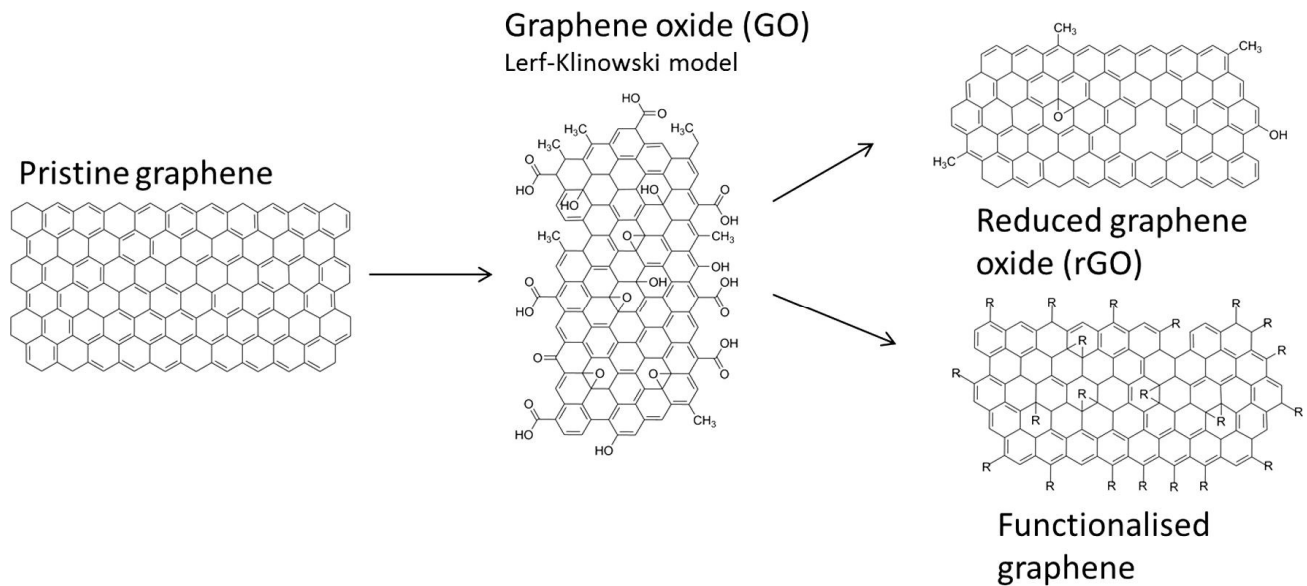


**Figure 1.** Structure of pristine graphene, GO, rGO, and functionalised graphene. Sourced and adapted with permission from Ref. [17].

In addition, graphene and graphene-based nanomaterials are extremely flexible in their ability for functionalisation and hybridisation, which is useful when tailoring nanomaterials for use in targeted tracking and/or treating diseased cells/tissues [18]. The high surface area, planar nature, and delocalised free  $\pi$ -electrons allow non-covalent modifications; the oxygen-containing groups that decorate the graphene surface are used for covalent modifications. Covalent modifications are most common for GO or rGO and involve agents, such as polyethylene glycol (PEG), folic acid (FA), or chitosan to increase the solubility and stability of the graphene derivative within physiological environments and solutions [19]. Non-covalent modifications utilise supramolecular interactions, such as  $\pi$ - $\pi$  stacking and hydrophobic interactions between graphene and coating molecules in order to increase the amphiphilicity of the nanomaterial, as well as the binding capacity, reactivity, biocompatibility, and sensing properties [19–21]. Non-covalent functionalisations include the use of polymers, biomolecules, drugs, and carbon nanoallotropes, which are important in reducing the cytotoxic effects of graphene nanomaterials [21].

Graphene and its derivatives have been extensively studied for their use in targeted and non-targeted drug delivery applications. Due to its exceptionally large surface area and aromatic structure, graphene has the potential for high drug loading capacity of various biomolecules and drugs, particularly aromatic drugs, through highly efficient  $\pi$ - $\pi$  stacking. Previous research in this area has mostly focused on graphene's use in the delivery of chemotherapeutics. Drugs, such as DOX, camptothecin, paclitaxel, and cisplatin, have been tested [22]. Table 1 shows a non-exhaustive list but highlights the variety in previous studies that have incorporated therapeutics onto graphene-based drug delivery vehicles.

**Table 1.** Graphene-based nanocarriers developed for drug delivery applications. Further examples have been discussed elsewhere [23–25].

Graphene-Based Nanomaterial	Functionalisation	Loaded Therapeutic	Efficacy Test	Stimuli Response	Reference
GO	Polyethylene-glycol (PEG)	DOX	A549	Glutathione (GSH)	[26]
NGO	PEG	DOX hydrochloride	HeLa	GSH	[27]
GO	Poly(vinyl alcohol) (PVA)	Camptothecin	MDA-MD-231	-	[28]
GO	PLA-PEG	Paclitaxel	A549	-	[29]
rGO	Gold nanoclusters	DOX	HepG2	-	[30]
GO	DNA	DOX	HeLa	ATP	[31]
GO	FA-PEG	Camptothecin	HeLa	pH	[32]
rGO	PEG-BPEI	DOX	PC-3, HeLa	GSH/NIR	[33]
GO	PEG	DOX	EMT6	pH	[34]
GOQD	FA-CH	DOX	A549,SH-SY5Y, MDA-MB 231	pH	[35]
GO	Integrin $\alpha_V\beta_3$ mono-antibody-PEI	DOX	U87 MG, MCF-7	pH	[36]
GO	CMC-HA-FI	DOX	HeLa	pH	[37]
GO	Fe <sub>3</sub> O <sub>4</sub> , FA	DOX	SK3	pH	[38]
GO	PEG, HN-1	DOX	OSCC (CAL-27, SCC-25)	pH	[39]

The ability to easily functionalise graphene and its derivatives offers versatility to the drugs that can be loaded, but also in terms of the targeting ligands that can be incorporated, increasing the specificity of targeted delivery [22]. Zhang et al. developed a GO functionalised with stabilising sulfonic acid groups and folic acid molecules that were covalently bound to the NGO surface. Both DOX and camptothecin were loaded with high efficiency through  $\pi$ - $\pi$  stacking and hydrophobic interactions, and exhibited high cytotoxicity to breast cancer cell line MCF-7 due to the FA receptors on their surface [22,40]. Alternatively, antibodies, peptides, and aptamers can be utilised as targeting agents for specific cancer cells. Li et al. have recently developed a GO nanocarrier loaded with DOX that was functionalised with PEG and the HN-1 peptide. The HN-1 peptide has been identified as a small peptide specific to oral squamous cell carcinoma that is able to penetrate tumour tissues. Thus, its incorporation resulted in the increased targeting of cancer cells compared to DOX@NGO-PEG, higher cellular uptake, and cytotoxicity towards oral squamous cell carcinoma cell lines SCC-25 and CAL-27 [39].

As suggested in Table 1, the most extensively researched chemotherapeutic for loading onto GO has been DOX. As DOX is a widely used chemotherapeutic and is efficacious in multiple tumour types, it is useful for in vitro studies. DOX (Figure 2) is an anthracycline antibiotic isolated from the bacterium *Streptomyces peucetius* var. *caesi* with molecular formula C<sub>27</sub>H<sub>29</sub>NO<sub>11</sub>. After clinical approval in 1963, it has been widely used as a chemotherapeutic in the treatment of solid tumours, including breast, ovarian, lung, and thyroid cancers, and haematological cancers, including leukaemia, as well as both Hodgkin's and non-Hodgkin's lymphoma [41,42]. The anthracycline structure, which includes aromatic rings and amino groups, enables DOX to be loaded with high efficiency to graphene and its derivatives through both  $\pi$ - $\pi$  stacking and electrostatic interactions [23].

DOX can be released from graphene nanocarriers via several different mechanisms, making it an ideal chemotherapeutic for extensive research. The development of graphene nanohybrids as drug delivery vehicles that can respond to release stimuli improves the targeting and specificity of drug delivery further. Smart nanocarriers can release loaded drugs via both internal or external stimuli, including but not limited to pH, temperature, chemical reactions, light, ultrasound, ROS, and magnetic fields [19].

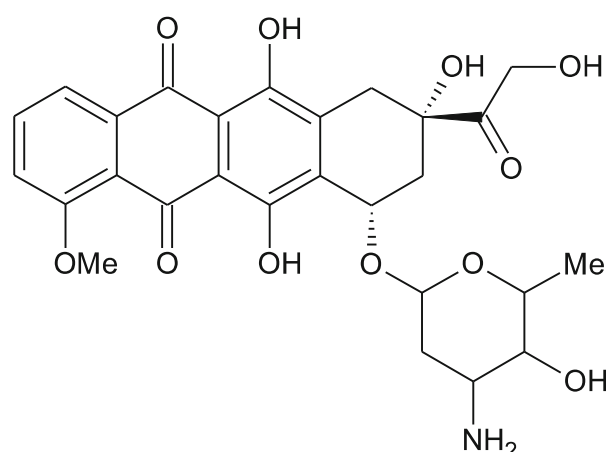


**Figure 2.** Chemical structure of DOX. Sourced with permission from Ref. [43].

The release of DOX by a pH-dependent response is one of the most common methods of release. Multi-functionalised GO with hyaluronic acid and the targeting Arg-Gly-Asp peptide, for example, utilised pH response and demonstrated that the cumulative release of DOX after 72 h at a pH of 5.5 was 30.2%, compared to 7.6% at a pH of 7.4 [44]. Delivery systems that pH-responsive are important in cancer treatment as acidic conditions (pH 5–6.5) are characteristic of tumour environments [20,45–47]. The low pH environment facilitates the protonation of DOX, which weakens the  $\pi$ - $\pi$  stacking and hydrophobic interactions between DOX and the nanocarrier, thereby facilitating the release of DOX from the graphene complex [25]. In addition, in a study using PEGylated GO, a more effective release of DOX was facilitated by treatment with glutathione (GSH) compared to the release from GO-PEG alone [23,26].

External stimuli have also been employed to release DOX from graphene nanocarriers, such as the work by Tang et al., who developed GO wrapped mesoporous silica NPs loaded with DOX that released DOX “on demand” under NIR laser irradiation [48]. Ma et al. worked on utilising GO decorated with iron oxide NPs and functionalised by PEG for the magnetically targeted drug delivery of loaded DOX. The application of an externally applied magnetic field resulted in the high uptake of GO-IONP-PEG-DOX by breast cancer cell line 4T1 directly within the applied field and the selective cytotoxicity to these cells by the released DOX, with the cells outside the magnetic field not affected [49].

The research effort into DOX-loaded graphene nanocarriers for drug delivery has been extensive and has seen a lot of progress in recent years; however, research is still limited to pre-clinical stages. Further, information on the release kinetics of DOX from different nanocarriers has not been studied; it is still unclear what the best release mechanism of DOX is for therapeutic efficacy. Understanding the most effective release of DOX from graphene nanocarriers may facilitate further focused research and accelerate the transfer of this technology to clinical applications. Driven by these needs, the current study aims to undertake a systematic review of the previous literature published on graphene-based drug delivery vehicles loaded with DOX for ovarian and breast cancer treatment, and analyse extracted data using mathematical models to identify the most successful and clinically relevant release mechanism. In addition, the limitations of published literature and any missing data are considered. In addition, recommendations for future work are addressed.

## 2. Materials and Methods

The protocol and methods followed were based on work done by Morgulchik and Kamaly [50].

### 2.1. Search Strategy, Inclusion, and Exclusion Criteria

Multiple library databases were used to accumulate the maximum number of appropriate publications available. PubMed<sup>®</sup>, Web of Science<sup>™</sup>, and OVID Medline<sup>®</sup> were the databases used in this study [50–53].

The following key terms were used to narrow down the search (“Graphene” OR “Graphene nanoparticle”) AND (“Doxorubicin” OR “DOX”) AND (“Breast Cancer” OR “Ovarian Cancer”) AND (“Drug Delivery” OR “Drug Release”). No date restrictions were applied, and all papers were required to be written in English. Publications that involved the use of graphene quantum dots (GQDs), publications that were based on quantum dot nanohybrids, publications that incorporated hydrogels, and publications that combined chemo- and photothermal therapy to use more than one type of release stimulation were excluded. Further, only publications with adequate drug release data and those that consistently used the correct cancer cell line for biological assays were included.

Immediately after the search was conducted, duplicate publications were manually removed. Studies were then excluded by both title and abstract based on if the topic was unrelated, if the use of graphene was unclear or minimal, if the nanocarrier had been loaded with multiple drugs or if the study was intended for a different cancer type and therefore used inappropriate cell lines. When analysing the eligibility of selected publications by the full text, records that were review papers, records that supplied insufficient quantitative data, records that used inappropriate cell lines, or records that did not supply the drug release profile within the main body of the report were excluded. No ethical approval or consent was required as all the data were extracted from published studies.

### 2.2. Study Characteristics

For each of the publications included in this research, the title, author, journal, publication date, and digital object identifier (DOI) were recorded. For the qualitative data extraction, the nanocarrier characteristics and the experimental conditions were recorded. The nanocarrier characteristics include the composition, basic method of fabrication, and physiochemical characteristics. The experimental conditions extracted include the payload characteristics, drug loading capacity/efficiency, pH, temperature, method of release, and the cell lines used in biological assays.

### 2.3. Data Extraction

The percentage of cumulative drug release over time for different stimuli responses (pH, NIR, Ultrasound) was extracted from the drug release profiles in each publication and recorded. The data was extracted using the GetData Graph Digitizer (version 2.26) [54].

### 2.4. Mathematical Modelling of In Vitro Drug Release

To study the release kinetics, the extracted drug release data from all 17 publications were fitted to four conventional drug release kinetic models described by Equations (1)–(4).

$$F = k_0 \cdot t \quad (1)$$

Equation (1) describes the zero-order model, where  $F$  is the fraction of the drug released at time  $t$  and  $k_0$  is the zero-order release rate constant. The amount of drug released plotted against time gives  $k_0$  as the gradient [55–58].

$$\ln(1 - F) = -k_1 \cdot t \quad (2)$$

Equation (2) describes the first-order model, where  $k_1$  is the first-order rate constant. By plotting the cumulative % drug remaining against time,  $k_1$  can be determined by the gradient [56–59].

$$F = k_H \cdot \sqrt{t} \quad (3)$$

Equation (3) describes the Higuchi model, where  $k_H$  is the Higuchi release rate constant, which is determined as the gradient when the amount of drug released is plotted against the square root of time [56–59].

$$\ln[-\ln(1-F)] = \beta \cdot \ln(t_d) + \beta \cdot \ln(t) \quad (4)$$

Equation (4) describes the Weibull model, where  $t_d$  is the lag time prior to drug release and  $\beta$  characterises the shape of the release curve. This model does not give fundamental release kinetic values and is used as a descriptive model to understand the release profile [55–57,60].

### Parameters

The goodness-of-fit of the models to the data was assessed using two statistical measures, the coefficient of determination,  $R^2$ , (Equation (5)), and by calculating the standard deviation of the residuals represented by the standard error of estimate  $Sy.x$  (Equation (6)).

$$R^2 = 1 - \frac{SS_{res}}{SS_{tot}} = 1 - \frac{\sum_i (y_i - \hat{y}_i)^2}{\sum_i (y_i - \bar{y})^2} \quad (5)$$

In this equation,  $SS_{res}$  is the residual sum of the squared errors, and  $SS_{tot}$  is the total sum of squared errors. The residual term  $y_i - \hat{y}_i$  represents the difference between the observed value,  $y_i$  and the predicted value,  $\hat{y}_i$ . Further,  $\bar{y}$  is the mean of the observed data [50].

$$Sy.x = \sqrt{\frac{\sum_i (\hat{y}_i - y_i)^2}{n - k}} \quad (6)$$

In this equation,  $n$  is the number of observations, and  $k$  is the number of parameters that are included in the regression [50,61].

The  $p$  value was also recorded to highlight the strength of the results with a small value, suggesting strong evidence behind the results [62]. All statistical analyses and model fitting were performed in GraphPad Prism version 9.1.2 (225) for Mac OS Catalina [63]. Methodological improvements and future considerations can be found in Supplementary Information.

## 3. Results and Discussion

### 3.1. Study Design

A systematic search of three library databases enabled the accumulation of previous publications that have incorporated DOX-loaded graphene nanocarriers for research into the response of breast and ovarian cancer cell lines. As illustrated by the search and inclusion flowchart (Figure 3) from the initial search, the study identified a total of 175 studies, 47 from PubMed®, 91 from Web of Science™, and 34 from Ovid Medline®; a further three were identified through referencing. Through combining the search engine's results, twenty-four publications were immediately excluded through duplication. Seventy records were then removed simply because their title did not adhere to the inclusion criteria; for example, those that were based on GQD nanohybrids, those that loaded more than one chemotherapeutic in addition to DOX, or those of an unrelated topic. A further thirty studies were removed through screening of the abstract, and thirty-four were removed through screening the full text. Commonly the excluded papers used an inappropriate cell line, incorporated multiple drugs, or provided insufficient drug release data.

Table S1 reports the title, first author, journal, date of publication, and DOI for the seventeen publications [44,64–79]. Those included were published in sixteen scientific journals ranging from 2008 to 2021. Of these, 65% were published within the last five years (since 2016), highlighting the advancement of research and research interest in the area of graphene nanomaterials for drug delivery.

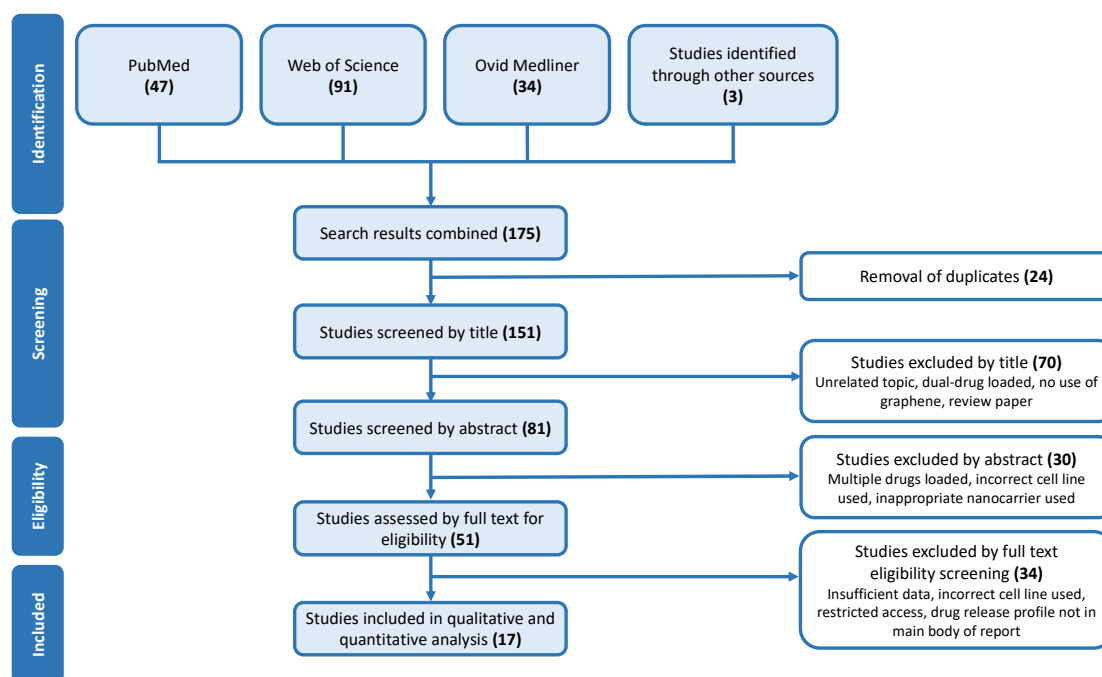


**Figure 3.** A systematic search and inclusion flowchart from the search engines PubMed<sup>®</sup>, Web of Science<sup>TM</sup>, and Ovid Medline<sup>®</sup>. Studies were all screened by title, abstract, and by full text to assess their eligibility. A total of seventeen studies were included for analysis based on the predefined inclusion and exclusion criteria.

The inclusion criteria excluded the use of publications that were based on QGDs and of those that incorporated the use of hydrogels. By limiting the studies to those based on 2D graphene and GO nanosheets, more comparisons can be drawn and evaluated. It should be highlighted that studies were excluded due to the inconsistent use of cancer cell lines and biological assays. Several studies incorporated the use of multiple cell lines but did not consistently represent them in all in vitro assays undertaken. These publications were therefore excluded due to inconsistencies in their experimental protocols and published results.

### 3.2. Nanocarrier Characteristics

The nanocarrier characteristics are summarised in Table S2. Of the publications analysed, 88% suggest cancer as the therapeutic application of the study with only two papers not suggesting an application. The size and shape of the nanohybrids varied widely throughout the publications due to the host of different nanohybrids involved; however, most publications recorded at least one of either the height/thickness or size of the system (although these measurements were ill-defined). The height or thickness recorded ranged from 0.8–144 nm, with nine studies reporting it only between 0.8–13 nm. The reported size of the nanocarriers ranged from 35–240 nm. Most papers also compared the size of the functionalised graphene nanocarriers against the size of a single layer GO sheet, which was typically recorded as being between 0.8–1.5 nm in height. The shape and morphology were also varied through the publications; the majority stated that the nanohybrid exhibited a rough surface compared to that of smooth pristine graphene due to the presence of functionalisation. The surface charge ranged from +17.9 mV to −39 mV; unfortunately, this parameter was unrecorded in 47% of studies.

In 88% of the studies, functionalised GO was used as the nanosystem. Functionalisation included the use of polymers, natural products, dendrimers, metals, and metal oxides. PEG was the most common polymer used; in addition, natural biodegradable and biocompatible polymers, such as hyaluronic acid (1), cellulose (1), chitosan (1), and dextran (1) were also used as functionalising agents. PEG was used in seven publications in combination with other modifications. PEG is a hydrophilic polymer that is used for functionalisation

to improve the biocompatibility, water dispersity, solubility, and targeting ability of the nanosystem; in addition, PEG offers high efficacy, non-toxicity, non-immunogenicity, and flexibility [67]. PEG is preferentially used over other polymers as it increases the stability of the nanosystem by reducing the risk of aggregation, opsonisation, and phagocytosis. The PEG chains form a voluminous hydrated cloud surrounding the NPs that sterically hinders their interaction with blood components and proteins, thereby facilitating an increase in circulation time by avoiding uptake by the reticuloendothelial system (RES) [79–82].

FA was used in three publications as an active targeting agent due to its ability to bind with high affinity to FA receptors (FR). FR are overexpressed in several different human carcinomas, particularly in ovary, breast, lung, and brain cancers [79].

Metals and metal oxide NPs were also used as functionalising agents, as they can make nanocarriers responsive to different stimuli. Iron oxide ( $\text{Fe}_3\text{O}_4$ ) NPs are superparamagnetic and can transform electromagnetic energy into heat, which can be used as a trigger for drug release; their incorporation into GO and chitosan microspheres facilitated the nanosystem response to NIR and ultrasound stimulus [73]. Similarly, gold NPs deposited on a GO surface were utilised for their strong absorbance in the visible to NIR region due to their surface plasmon resonance effect in a system that utilised NIR as the release stimulus [78]. Furthermore, some of the publications that utilised pH response as the stimulus also incorporated metals or metal oxides into the nanosystem, offering the opportunity to use combined photothermal and chemotherapy.

### 3.3. Experimental Conditions

#### 3.3.1. Payload Characteristics and Drug Loading

Following the predefined inclusion criteria, all of the analysed studies were those that used the small molecule chemotherapeutic drug DOX as the payload (Table S3). The drug loading content (DLC) reflects the amount of loaded drug compared to the mass of the nanocarrier. The drug loading efficiency (DLE), on the other hand, reflects the amount of drug loaded on the nanocarrier against the amount of drug provided to the system; both parameters are recorded in Table S3.

The DLC ranges from 9.26–346%, and the DLE ranges from 50.0–99.7%. It was expected that of the two, the DLE would be higher, as it is often harder to obtain a high loading content [83]. This is the case for 71% of papers that recorded both parameters. For GO-PAC/HEC, however, the increase in the ratio of DOX to GO causes an increase in DLC from 49% at a ratio of 1:0.5 GO:DOX to 216% at a ratio of 1:4; a decrease in the DLE from 98% at 1:0.5 to 54% at the ratio of 1:4 was also observed [64]. Similar results were recorded for the NGO-HDex nanohybrid, which also exhibited a higher DLC to drug embedding efficiency [71]. Unfortunately, only 41% of the publications reported both the DLC and the DLE, although all publications reported at least one parameter.

These data offer examples of high DLC and high DLE of DOX onto the graphene-based nanocarriers. This outcome can be attributed to the high surface area of graphene and its derivatives. In addition, the aromatic structure of DOX facilitates the  $\pi$ - $\pi$  stacking onto graphene. Moreover, the functional groups on both DOX and GO allow strong hydrogen bonding to occur. The range in different loading efficiencies throughout the publications can be attributed to the variety of functionalisation methods that were used. It has been reported that functionalisation can either help or hinder the loading efficiency of a drug onto a nanocarrier. A compromise must be met between keeping a relatively high loading efficiency but also using a functional, non-toxic, and biocompatible nanocarrier.

The Zn-d 3-rGO nanohybrid offers a high loading efficiency of 99.7%, which may be attributed to the presence of  $\text{Zn}^{2+}$  and the formation of a complex between this positive Zn ion and the -O-H and -O groups on DOX; the complex traps DOX onto the nanocarrier, in addition to hydrogen bonding and  $\pi$ - $\pi$  stacking of DOX with GO [68]. Karimi and Namazi suggested that the presence of PEG in their GO-TD- $\text{Fe}_3\text{O}_4$ @PEG prevented the diffusion of DOX into the solution, thereby facilitating high loading efficiency in addition to electrostatic interactions,  $\pi$ - $\pi$  stacking, hydrogen bonding, and hydrophobic interactions [67].

On the other hand, the loading efficiencies of the two non-functionalised GO nanosystems were high, at 93.6% and 91% [72,77]. It has been suggested that the presence of functionalisation groups on graphene nanocarriers can hinder the loading efficiency of DOX due to their bulkiness [84]. Further supporting this, Guo et al. showed that the GO-HA-RGD/DOX nanosystem had a DLE of 72.9% compared to GO/DOX and GO-HA/DOX, which had loading efficiencies of 90.1% and 76.3%, respectively [44].

### 3.3.2. Drug Release

The drug release conditions and maximum cumulative drug release for each of the publications are shown in Table S4. The temperature for in vitro drug release experiments was consistently kept at 37 °C, excluding three papers where the temperature was not recorded. The pH varied between the range of 2–10 between publications; however, drug release was most consistently recorded under (a) pH 7 or 7.4, which aims to represent cell surface or cytosolic neutral pH, or (b) a more acidic pH of 5.0–5.4, which reflects the lysosomal pH.

Sixteen of the analysed publications show a controlled release of DOX from the nanocarrier over a period greater than twenty-four hours. One of the main target functions of a nanocarrier is to provide controlled release of the loaded drug. This functionality is important as a controlled system aims to reduce toxic side effects as compared to burst release by prolonging therapeutic efficacy, maintaining optimal concentrations, preventing degradation, and preventing fluctuations in concentrations [85]. A nanocarrier is also responsible for delivering the loaded drug to the target site. All of the analysed publications show a stimuli-responsive release of DOX from the nanocarriers, with fifteen studies being responsive to pH and two studies being stimulated by either NIR or ultrasound. With the presence of a stimulus, the amount of drug released is significantly increased. For example, the nanohybrid GO-PAC/HEC showed a release of 80% at pH 5.0 after 35 h; in contrast, 20% of the loaded drug was released after 35 h at pH 7.4 [64]. The increased release in acidic conditions is attributed to the partial dissociation of the hydrogen bonding between DOX and GO [72].

Under neutral conditions, DOX can form four hydrogen bonds with a GO sheet through the -COOH and -OH functional groups on GO and the -NH<sub>2</sub> and -OH group on DOX. Under acidic conditions, the DOX becomes protonated, changing the -NH<sub>2</sub> to an -NH<sub>3</sub><sup>+</sup> group that cannot partake in hydrogen bonding. The hydrogen bonding strength is lower under acidic conditions, thereby increasing the hydrophilicity and solubility of DOX and facilitating its release [36,64,67]. pH-responsive nanocarriers are useful in cancer research as tumour microenvironments have an acidic pH [50]. This acidity can be utilised to trigger intratumoural release of drugs from nanocarriers by taking advantage of specific surface chemistry interactions [65].

The GO-TD-Fe<sub>3</sub>O<sub>4</sub>@PEG/DOX nanohybrid showed the most successful release of DOX, with 97.3% being released after 72 h at a pH of 5.0 [67]. Of the publications that use a pH response to monitor drug release, 73% show that more than half of the maximum cumulative release occurs in a controlled manner within the first twelve hours. This outcome may be attributed to the initial breaking of hydrogen bonding between the polar groups of DOX and the nanocarrier; the  $\pi$ - $\pi$  stacking interactions are responsible for the observation of continued release throughout the time frame [75]. Typically, the publications that did not show this rapid initial DOX release were those that measured release over longer time frames. It should be highlighted that several publications demonstrate a high drug release at neutral conditions. The nanohybrids Zn-d3-rGO and FA-BSA/GO release over half of the loaded drug without any stimuli, thereby suggesting that less than half of the DOX loaded will reach the target site [50,68,70].

Alternatively, NIR- and ultrasound-stimulated release enhance the delivery of DOX from graphene nanocarriers through the absorption of energy. NIR release is used due to the high NIR absorbance of graphene and its derivatives; through light absorption and photothermal conversion, the loaded drug is released. The release can be enhanced by

the incorporation of other NPs. In GO@Ag-DOX-NGR, the NIR irradiation causes the excitation of electrons from Ag, which due to conjugation results in the hydrolysis of the ester linkage between DOX and the nanocarrier [78,86,87]. Li et al. investigated the drug release under stimulation from NIR and ultrasound. DOX release was controlled under normal conditions; when exposed to stimulation of either NIR or ultrasound, the release rate jumped due to the burst release of DOX that was caused by the sudden increase in energy [73].

Light-mediated drug release by UV or visible light has drawbacks due to the inadequate tissue penetration and potential phototoxicity. Stimulation by NIR is thought to be superior in both aspects due to the longer wavelength(s) of light used (700–1000 nm). Recent evidence has suggested that cancer microenvironments can not only have an acidic environment but can also be alkaline, which is associated with limitations to drug release by an acidic pH [88]. The combination of pH and NIR stimulated response may be the most efficacious in the future as a theragnostic technique.

### 3.4. Mathematical Modelling of Drug Release Kinetics

The use of mathematical models enables the evaluation of the drug release process under different conditions and can aid in understanding the mechanism of release whether it be diffusion controlled, chemically controlled, osmotically controlled, or swelling and/or dissolution controlled; models can elucidate the main determinants to the rate of this release [55,89]. Mechanistic models accurately and reliably describe drug release systems; however, they are complex models that incorporate multiple parameters and require large quantities of experimental data. The use of empirical models is more widespread as they incorporate only a few parameters and are simpler to interpret. In addition, they are more tolerant of experimental variation, and are largely applicable on the nanoscale. The use of empirical models is, however, less performant due to the associated assumptions [50,90]. It is important to understand and to be able to predict the release behaviour of drug delivery systems in different conditions *in vitro* prior to further development. This enables the design and formulation of nanocarriers that are associated with optimal drug release and delivery [60].

This study uses four models to analyse the kinetic release data of DOX from the loaded nanocarriers. The zero-order model describes the drug release at a constant rate of time, in which the drug release rate is not dependent on the amount of drug remaining. Zero-order kinetics are best used to describe drug release from transdermal systems and low dosage matrix tablets; it is rare for complex nanocarriers to follow a zero-order release [50,91].

The first-order model describes a system where the rate of release is dependent on the concentration of the remaining drug and has been used to describe absorption and elimination of some drug formulations, particularly water-soluble drugs [55,92]. The Higuchi model is one of the most used models to describe the release rate from matrix systems and can be applied to planar systems as well as those with different geometries and porous structures [60,93]. By using the Higuchi equation, the assumptions of its derivation must be considered which makes it rarely applicable for many controlled release systems, stimuli-responsive swellable matrices, and nanogels smaller in dimension than their payload [50]. Assumptions include “The initial drug concentration in the system is much higher than the solubility of the drug, mathematical analysis is based on 1D diffusion and thus, edge effects must be negligible, the suspended drug is in a fine state such that the particles are much smaller in diameter than the thickness of the system, swelling or dissolution of the polymer carrier is negligible, the diffusivity of the drug is constant and perfect sink conditions are maintained” [93].

Finally, the Weibull model is commonly used for comparing the release profiles of matrix-based systems and is useful due to its flexibility in fitting to experimental data [58,92]. Due to this flexibility and the sensitivity of its parameters, the Weibull model has been applied to both rapid release systems and extended drug delivery systems [55]. The Weibull model has two parameters:  $t_d$  is the lag time before the onset of drug release,

and the parameter  $\beta$  is a shape parameter that describes the shape of the release curve. When  $\beta = 1$ , it implies an exponential drug release profile; if  $\beta > 1$ , the release profile is sigmoidal. If  $\beta < 1$ , the graph is parabolic [58]. This model infers a descriptive account of a drug release profile but does not describe any dissolution kinetic properties. Further, it has limited use for establishing both in vitro and in vivo correlations [60,91].

The calculated regression coefficient,  $R^2$  has been calculated for all experimental conditions for each of the analysed publications (Table 2). The  $R^2$  value is a measure of the goodness-of-fit of a set of data to a particular model and ranges from 0 to 1;  $R^2$  tending closer to 1 represents a greater goodness-of-fit and suggests the drug release kinetics can be described by that model. The standard error of estimate,  $Sy.x$ , the gradient, and the  $p$  value for each nanohybrid at different conditions have also been recorded and are displayed in Table S5. The linear regression graphs for each publication that the results are based upon can be found in Figures S1–S17.

**Table 2.** The goodness-of-fit parameter  $R^2$  reported for the nanocarrier and different release conditions in each publication for four kinetic models.

Paper	Nanocarrier and Release Condition	Zero-Order	First-Order	Higuchi	Weibull
		$R^2$	$R^2$	$R^2$	$R^2$
1	GO-HA-RGD (pH 5.5)	0.8597	0.8746	0.9422	0.9611
	GO-HA-RGD (pH 7.4)	0.7367	0.7390	0.8464	0.8996
2	GO-PAC/HEC (pH 5.0)	0.6516	0.7768	0.8431	0.9694
	GO-PAC/HEC (pH 7.4)	0.6231	0.6409	0.8261	0.9502
	NGO-PEG-DA (pH 5.0)	0.7288	0.7710	0.8783	0.8823
3	NGO-PEG-DA (pH 6.8)	0.9860	0.9869	0.9609	0.9720
	NGO-PEG-DA (pH 7.4)	0.3289	0.3297	0.4790	0.6881
	NGO-PEG-SA (pH 5.0)	0.8149	0.8389	0.9244	0.9273
	NGO-PEG-SA (pH 6.8)	0.9118	0.9177	0.9498	0.9488
	NGO-PEG-SA (pH 7.4)	0.4873	0.4875	0.6830	0.8610
4	GO-PEG-SS-HY (pH 5.5)	0.7834	0.8080	0.9150	0.9451
	GO-PEG-SS-HY (pH 7.4)	0.8061	0.8158	0.9304	0.9309
5	GO-TD-Fe <sub>3</sub> O <sub>4</sub> -PEG (pH 5.0)	0.8382	0.9618	0.9327	0.9817
	GO-TD-Fe <sub>3</sub> O <sub>4</sub> -PEG (pH 6.8)	0.8707	0.9491	0.9539	0.9762
	GO-TD-Fe <sub>3</sub> O <sub>4</sub> -PEG (pH 7.4)	0.8600	0.9315	0.9453	0.9708
6	Zn-d-3 rGO (pH 5.4)	0.9085	0.9652	0.9846	0.9870
	Zn-d-3 rGO (pH 7.4)	0.8866	0.9137	0.9689	0.9749
	GO (pH 5.4)	0.5447	0.5871	0.7012	0.7854
	GO (pH 7.4)	0.4561	0.4868	0.6016	0.6859
7	GO/(PHEMA-g-PLA)-b-PEG-b-(PHEMA-g-PLA) (pH 5.4)	0.8553	0.8972	0.9515	0.9830
	GO/(PHEMA-g-PLA)-b-PEG-b-(PHEMA-g-PLA) (pH 7.4)	0.5818	0.6073	0.7737	0.9155
8	FA-BSA/GO (pH 5.0)	0.7846	0.8607	0.9091	0.9772
	FA-BSA/GO (pH 7.4)	0.9032	0.9427	0.9747	0.9754
9	NGO-HDex (pH 5.5)	0.9624	0.9755	0.9975	0.9982
	NGO-HDex (pH 7.4)	0.9914	0.9942	0.9909	0.9892
10	GO (pH 2)	0.8323	0.9360	0.9322	0.9123
	GO (pH 7)	0.5794	0.5928	0.7161	0.6499
	GO (pH 10)	0.6437	0.6752	0.7846	0.7796
11	Fe <sub>3</sub> O <sub>4</sub> /GO/Chitosan (Normal Release)	0.9845	0.9958	0.9990	0.9877
	Fe <sub>3</sub> O <sub>4</sub> /GO/Chitosan (NIR assist)	0.9429	0.9643	0.9690	0.9337
	Fe <sub>3</sub> O <sub>4</sub> /GO/Chitosan (Ultrasound assist)	0.9221	0.9464	0.9538	0.9096
12	PF127/GN (pH 5)	0.6961	0.7494	0.8444	0.8964
	PF127/GN (pH 7)	0.5976	0.6186	0.7643	0.7734
	PF127/GN (pH 9)	0.6758	0.7080	0.8405	0.8397
13	GO-A-Im (pH 3.4)	0.5645	0.6732	0.7116	0.8374
	GO-A-Im (pH 5.4)	0.6178	0.7175	0.7600	0.8626
	GO-A-Im (pH 7.4)	0.5040	0.5113	0.6534	0.8166

Table 2. Cont.

Paper	Nanocarrier and Release Condition	Zero-Order	First-Order	Higuchi	Weibull
		$R^2$	$R^2$	$R^2$	$R^2$
14	GO-PEG-FA-SH (pH 4)	0.9831	0.9920	0.9983	0.9911
	GO-PEG-FA-SH (pH 7.4)	0.9473	0.9542	0.9902	0.9958
	GO-PEG-FA/GNPs (pH 4)	0.9906	0.9975	0.9970	0.9872
	GO-PEG-FA/GNPs (pH 7.4)	0.9899	0.9943	0.9948	0.9786
15	GO (pH 5)	0.9360	0.9440	0.9887	0.9976
	GO (pH 7.2)	0.7671	0.7705	0.9034	0.9491
	GO (pH 9)	0.8733	0.8778	0.9597	0.9742
16	GO@Ag (NIR laser)	0.9674	0.9868	0.9931	0.9885
	GO@Ag (No NIR laser)	0.9909	0.9912	0.9831	0.9943
17	GO-PEG-Fol (pH 5.5)	0.8911	0.9003	0.9735	0.9933
	GO-PEG-Fol (pH 7.4)	0.9944	0.9947	0.9636	0.9220

The Weibull Model showed a higher degree of correlation coefficient for 69% of the nanocarriers under any release condition, with  $R^2$  values ranging from 0.7734 to 0.9982. This suggests that, although the pH affects the rate of release, the mechanism of drug release is the same. Interestingly, compared to the systems that are governed by pH stimulated release, drug release that has been stimulated by NIR or ultrasound shows the highest degree of correlation towards the Higuchi model with  $R^2$  values as high as 0.9990, suggesting that these systems are governed by a diffusion-based drug release [91]. It should be noted that two conditions displayed anomalous results and were excluded from further evaluation; these are highlighted in red in Table 2.

The  $p$  values were recorded to evaluate the strength of the results; a smaller  $p$  value suggests a lower probability that the data could randomly produce a linear regression like that observed. Most data show a  $p$  value below 0.05, suggesting significant findings. The only non-significant results were recorded for NGO-PEG-DA at pH 7.4 [65]; this experimental condition also showed low  $R^2$  values, highlighting its anonymity from the rest of the data.

The standard error of estimate,  $Sy.x$  is another statistical measure that validates the goodness-of-fit of the data to a specific model. For better fit results, the value of  $Sy.x$  will be small. The  $Sy.x$  is consistently the smallest for the first-order model in most publications closely followed by the Weibull model. The  $Sy.x$  values for the zero-order and Higuchi models were significantly higher, suggesting a large deviation of the residuals. This is unsurprising as the zero-order model has the least correlation to any of the nanohybrids and rarely describes release from complex nanocarriers.

The release constant for the zero-order ( $k_0$ ), first-order ( $k_1$ ), and Higuchi model ( $k_H$ ) as well as the  $\beta$  value for the Weibull Model were recorded by extracting the linear regression gradients. These are significant as they describe the rate of DOX release from the system. The values for  $k_0$ ,  $k_1$ , and  $k_H$  are greatest, at pH 5/5.5, compared to pH 7/7.4 in all of the pH stimulated systems. The release rate also tends to be slightly higher at a more basic pH compared to a neutral pH. These results are expected due to the partial dissociation of hydrogen bonds at both acidic and basic conditions.

### 3.5. Biological Assays

#### 3.5.1. Cytotoxicity

Of the publications analysed, 88% used biological assays to assess the cytotoxicity of the nanohybrids against either ovarian cancer cell lines (2) or breast cancer cell lines (13). Studies included the assessment of cell viability with the unloaded nanocarrier, as well as the DOX-loaded composite, to assess the biocompatibility. Graphene itself has been shown to be a relatively safe biomaterial yet has a time, concentration, size, and shape-dependent toxicity [24,94]. As mentioned previously, functionalisation can greatly improve the biocompatibility of the nanocarrier; in general, the results show the unloaded

nanocarriers were not toxic to normal or cancerous cells. In addition, the DOX-loaded nanocarriers showed increased cytotoxicity towards breast and ovarian cancer cell lines compared to free DOX.

The different cell lines used are displayed in Table S4; they included ovarian cancer cells SKOV-3, and breast cancer cell lines including MCF-7 and MDA-MB-231. In several publications, DOX-resistant MCF-7 cells were also utilised to understand if the DOX-loaded nanocarrier was more efficacious than free DOX against resistant cell lines.

Only 20% of the papers used *in vivo* experiments to assess cytotoxicity. These studies used mice to evaluate the tumour-killing efficiency of the DOX-loaded nanocarriers. Each of these three studies showed that the introduction of the nanocarrier with the loaded drug accumulated at the tumour site and efficiently suppressed the growth of the tumour. Further *in vivo* studies throughout the publications would be beneficial for understanding the cytotoxicity in living systems and enhancing the clinical translatability.

### 3.5.2. Cellular Uptake and Intracellular Localisation

The cell membrane employs different mechanisms to exchange substances, including passive and active transport as described previously. Endocytosis is a type of active transport and is where the cell engulfs external objects inside the extracellular fluid. Endocytosis is employed when NPs cannot pass through by passive transport due to either the size, charge, or polarity of the nanoparticle [95,96]. Twelve of the publications evaluated the cellular uptake of DOX into ovarian or breast cancer cell lines by means of fluorescent visualisation. Of these studies, 75% suggested that the mechanism of cellular uptake was endocytosis. The fact that DOX is intrinsically fluorescent negates the need for additional fluorescent probes. This is beneficial, as introducing additional elements to the nanocarrier increases the complexity and decreases the clinical translatability [71].

The mechanism of endocytosis employed in each of the studies will be dependent on the size, shape, surface charge, surface hydrophobicity, and functionalisation of nanocarriers. Folic acid is utilised in several publications for enhanced targeting, as it facilitates endocytosis through FR-mediated endocytosis. Ma et al. evaluated the uptake of DOX in MCF-7 cells with high levels of FR and human non-small-cell lung cancer cell line A549, which lack FR. The difference in uptake of FA-BSA/GO/DOX compared to the non-specific BSA/GO/DOX was significant in the MCF-7 cells, but was similar when incubated with A549 cells; thereby suggesting the folate-mediated endocytosis [70]. Alternatively, Guo et al. demonstrated specific cellular uptake of the nanohybrid GO-HA-RGD through both antigen and integrin binding. HA can specifically bind to the overexpressed antigen CD44 on the surface of tumour cells. In addition, the RGD targeting peptide recognises specific integrins on the tumour cell surface. The synergic effect of CD44-HA and Integrin-RGD mediated endocytosis facilitates the successful uptake into SKOV-3 cells [44].

By utilising receptor-mediated endocytosis and antibody-mediated endocytosis, the specificity of cellular targeting and subsequent uptake is improved. In living systems, off-target cells that are diseased or damaged may also have an acidic pH, be hypoxic, or be inflamed like the target cancer cells. Receptor- or antibody-mediated endocytosis reduces the chance of cellular uptake by non-specific target cells.

Sub-cellular targeting and intracellular localisation of graphene and its derivatives have not been extensively explored. It is important to understand where the DOX-loaded graphene nanocarrier accumulates within the cell and to identify if any functional groups elicit any specific targeting of intracellular organelles. Most of the publications suggested that the DOX accumulates in both the nucleus and cytoplasm, although the localisation was not comprehensively studied throughout. There is most likely a high accumulation of DOX in the nuclei of cells due to the high affinity it has for DNA [77]. In addition, Han et al. functionalised a graphene nanocarrier with hypericin, a mitochondria-targeting ligand, and found it to elicit an anti-tumour effect by inducing the mitochondria-mediated apoptosis pathway [66].

### 3.6. Clinical Relevance

The development of drug nanocarriers still faces large challenges in moving from bench to bedside, including issues related to efficacy, toxicity, biocompatibility, biodegradability, and clearance/excretion pathways. Some of the main issues are related to large-scale production and quality assurance. Large-scale production of graphene requires the re-production of materials with the same size, polydispersity, morphology, charge, surface modifications, and stability, all whilst maintaining and adhering to regulatory standards. This is extremely difficult to achieve and requires extensive infrastructure, expertise, technology, and money [97].

More specifically for drug delivery devices, one of the major translational barriers of *in vitro* and *in vivo* studies to clinical use is understanding the accumulation amount of the drug at the target site and whether *in vitro* studies are representative of drug concentrations that would be relevant in clinical applications. The advised clinical dosage of DOX in chemotherapy is 60–75 mg/m<sup>2</sup> over a course of 3 to 10 min every 21 days. This is dependent on the dosage regimen, type of cancer, stage of cancer, and any previous treatment or combined treatments that the patient has undergone [98,99]. The analysed publications do not address the overall delivery efficiency of DOX to the target site or the absolute accumulation of DOX within the cell; this is mainly due to the fact that the majority are limited to proof-of-concept *in vitro* studies.

The GO-TD-Fe<sub>3</sub>O<sub>4</sub>@PEG composite, records a high DLE of DOX at 92.6% and a high cumulative release of 97.3% at pH 5.0 after 72 h, suggesting high delivery efficiency [67]. Whereas GO-PEG-FA/GNPs/DOX has a high loading efficiency of 84%, only ~43% of that loaded drug is released at pH 4.0 after 295 h [76]. Finally, NGO-PEG-DA/DOX has a reasonably low loading efficiency of 50% and only releases 31.4% of that loaded drug after 24 h [65], which theoretically means that if 1 mg of DOX was loaded onto the nanohybrid, only 0.157 mg would reach the intended target. These data suggest that the amount of DOX reaching the target site can be extremely varied and often may require a higher initial dosage to account for the loss. Future research should focus on using clinically relevant concentrations of DOX in pre-clinical experiments and accurately report on the delivery efficiency of the drug to evaluate the efficacy of nanocarriers.

In addition, the timeframe of action of the drug-loaded nanocarrier is important to understand in order to translate to clinical use. The timeframe through which the maximum cumulative release of DOX was measured varied drastically through the publications. Four of the analysed studies recorded the drug release profile over a period of more than six days, with one publication recording results up to thirteen days after initial release. It is questionable why the drug release was recorded for this long and whether this is clinically relevant or translatable to chemotherapy within this timeframe as the drug-loaded nanocarrier may be cleared from the body under physiological conditions. The terminal half-life for free DOX, for instance, is only 20–30 h [100]. Research should be undertaken to understand the optimum time frame for drug release to the specific target for maximum efficacy and to evaluate the retention time of graphene nanocarriers within the target site.

### 3.7. Recommendations for Future Work

The targeting of mitochondria and the subsequent induction of mitochondria-mediated apoptosis is an emerging pharmacological target. The mitochondrion is considered to be the ‘powerhouse’ of the cell; it generates cellular energy, is required for oxidative phosphorylation, adenosine triphosphate (ATP) production, ROS production, and cell cycle control. Consequently, the dysfunction of mitochondria disrupts these crucial energetic processes and causes cell apoptosis, autophagy, and necrosis [3,66]. Mitochondria-targeting nanocarriers may eliminate the need for photothermal therapy in addition to chemotherapy in the future which is already limited due to the hypoxic environment of cancer cells and its need for oxygen.

As discussed previously, of the publications analysed, very few clearly investigated the subcellular localisation of the drug-loaded nanocarrier after cellular uptake; although

mitochondria-targeting is an emerging area of interest in cancer therapy, only one publication highlighted its relevance and introduced a mitochondria-targeting ligand. Further, the localisation of graphene and its derivatives within the cell is still unknown. Future research should identify the subcellular localisation of graphene nanocarriers and aim to incorporate mitochondria-targeting ligands in order to induce cancerous cell apoptosis more efficiently, safely, and with less toxic effects to normal cells [3].

It would also be beneficial for future work to have standardisation for the minimal information needed to be recorded to eliminate incomplete data reporting [83]. In addition, standardisation of synthesis routes, raw materials and chemicals used in the synthesis, and the concentrations of both DOX and graphene used, should be considered. Future research may also benefit from the identification of whether the drug-loaded graphene nanocarriers adhere to standardised parameters, such as those defined by Lipinski in 2001. Lipinski defined five parameters for drug-like compounds that describe ideal physiochemical properties. These guidelines state that poor absorption or permeation are more likely to occur when the molecular mass is over 500 Da, there are more than five hydrogen-bond donors, more than ten hydrogen-bond acceptors, and the water-octanol partition coefficient (logP) is over five. Biological substrates are defined as exceptions to the rule [3,101].

Another major limitation to this research is that the long-term biodistribution and clearance pathways of the nanocarriers have not been clearly highlighted throughout the analysed publications. It is important to understand the clearance pathway of the nanocarrier system as well as to evaluate its long-term biocompatibility and toxicity. Most of the publications analysed only basic *in vitro* experiments; more complicated *in vivo* studies have not yet been reached. To understand the clearance pathways of the nanocarrier from a living system, *in vivo* or human studies must take place.

#### 4. Conclusions

This study focused on identifying and analysing previously published research on DOX-loaded 2D graphene nanohybrids for the treatment of ovarian and breast cancers with the aim of then understanding the relationships between different nanocarriers and *in vitro* drug release parameters. Although there are a host of different proof-of-concept publications of graphene-based nanocarriers, there have been no studies that focus on the systematic evaluation of graphene nanocarriers as a whole and their drug release efficiencies. Seventeen publications were identified, which utilised either pH or NIR/ultrasound to stimulate DOX release; both qualitative and quantitative data were analysed. By use of the programmes GetData and GraphPad Prism, the drug release profiles were extracted and fitted to four known kinetic models as drug release kinetics offers information that can be used to optimise nano delivery systems. It was found that most of the publications best fit the Weibull model, highlighting both the flexibility of the model to describe a range of different systems and the agreement between previous publications. This provides a predictable estimation of DOX release from graphene-based nanocarriers that can aid in the future development of drug delivery systems. The qualitative data extraction of this work unearthed inconsistencies of parameters reported between publications; a standardisation of information reporting could overcome this limitation and make further analysis more accurate. Future work should also focus on the development of *in vitro*/*in vivo* methods that can more accurately replicate physiological conditions; the use of computational modelling prior to pre-clinical experiments may aid in this translation. Future methods should take into consideration clinical relevance and translatability, cytotoxicity, cellular uptake, intracellular localisation, and the breakdown and clearance pathways of the nanocarriers.

**Supplementary Materials:** The following are available online at <https://www.mdpi.com/article/10.3390/app112311151/s1>, Figures S1–S17, the linear regression graphs of the zero-order, first-order, Higuchi, and Weibull models for each of the seventeen publications analysed. The equation of the linear regression is displayed as well as the  $R^2$  value for each model under each condition, Table S1: Table displaying the title, first author, journal, publication year and DOI for the seventeen publications analysed, Table S2: Table displaying the nanocarrier characteristics of each of the

seventeen publications analysed, Table S3: Table displaying the payload characteristics and drug loading information, including both the drug loading capacity and drug loading/encapsulation efficiency, for the seventeen publications, Table S4: A table displaying the experimental conditions under which the drug release was recorded, including the temperature and pH. The maximum cumulative release and the timeframe of the measurement were recorded. Information on the biological assays undertaken by each publication is also recorded, Table S5: This table displays the numerical results of the statistical analysis. The  $R^2$  value,  $Sy.x$  value, gradient, and  $p$  value are recorded for each of the four kinetic models, for each nanohybrid under the different conditions recorded by the publications. The results are given to 4 decimal places.

**Author Contributions:** Conceptualization, T.A.T., K.T. and R.J.N.; methodology, K.T.; validation, K.T., T.A.T. and R.J.N.; formal analysis, K.T.; investigation, K.T.; writing—original draft preparation, K.T.; writing—review and editing, K.T., T.A.T. and R.J.N.; supervision, T.A.T. All authors have read and agreed to the published version of the manuscript.

**Funding:** This research received no external funding.

**Institutional Review Board Statement:** Not applicable.

**Informed Consent Statement:** Not applicable.

**Data Availability Statement:** Not applicable.

**Conflicts of Interest:** The authors declare no conflict of interest.

## References

1. Cancer. Available online: [https://www.who.int/health-topics/cancer#tab=tab\\_1](https://www.who.int/health-topics/cancer#tab=tab_1) (accessed on 23 August 2021).
2. Sung, H.; Ferlay, J.; Siegel, R.; Laversanne, M.; Soerjomataram, I.; Jemal, A.; Bray, F. Global Cancer Statistics 2020: GLOBOCAN Estimates of Incidence and Mortality Worldwide for 36 Cancers In 185 Countries. *CA A Cancer J. Clin.* **2021**, *71*, 209–249. [[CrossRef](#)] [[PubMed](#)]
3. Tabish, T.A.; Hamblin, M.R. Mitochondria-Targeted Nanoparticles (Mitonano): An Emerging Therapeutic Shortcut for Cancer. *Biomater. Biosyst.* **2021**, *3*, 100023. [[CrossRef](#)]
4. Tabish, T.A.; Narayan, R.J. Mitochondria-targeted graphene for advanced cancer therapeutics. *Acta Biomater.* **2021**, *129*, 43–56. [[CrossRef](#)] [[PubMed](#)]
5. Tabish, T.A.; Hamblin, M.R. Multivalent nanomedicines to treat COVID-19: A slow train coming. *Nano Today* **2020**, *35*, 100962. [[CrossRef](#)]
6. Tabish, T.A.; Zhang, S.; Winyard, P.G. Developing the next generation of graphene-based platforms for cancer therapeutics: The potential role of reactive oxygen species. *Redox Biol.* **2018**, *15*, 34–40. [[CrossRef](#)] [[PubMed](#)]
7. Tabish, T.A.; Narayan, R.J. Crossing the blood–brain barrier with graphene nanostructures. *Mater. Today* **2021**, in press. [[CrossRef](#)]
8. Langer, R.; Weissleder, R. Nanotechnology. *JAMA* **2015**, *313*, 135. [[CrossRef](#)]
9. Definition-Nanomaterials-Environment-European Commission. Available online: [https://ec.europa.eu/environment/chemicals/nanotech/faq/definition\\_en.htm](https://ec.europa.eu/environment/chemicals/nanotech/faq/definition_en.htm) (accessed on 23 August 2021).
10. Soares, S.; Sousa, J.; Pais, A.; Vitorino, C. Nanomedicine: Principles, Properties, and Regulatory Issues. *Front. Chem.* **2018**, *6*, 1–15. [[CrossRef](#)]
11. Khan, I.; Saeed, K.; Khan, I. Nanoparticles: Properties, Applications and Toxicities. *Arab. J. Chem.* **2019**, *12*, 908–931. [[CrossRef](#)]
12. Yetisgin, A.; Cetinel, S.; Zuvun, M.; Kosar, A.; Kutlu, O. Therapeutic Nanoparticles and Their Targeted Delivery Applications. *Molecules* **2020**, *25*, 2193. [[CrossRef](#)]
13. Anselmo, A.; Mitragotri, S. Nanoparticles in The Clinic: An Update. *Bioeng. Transl. Med.* **2019**, *4*, e10143. [[CrossRef](#)] [[PubMed](#)]
14. Bobo, D.; Robinson, K.; Islam, J.; Thurecht, K.; Corrie, S. Nanoparticle-Based Medicines: A Review of FDA-Approved Materials and Clinical Trials to Date. *Pharm. Res.* **2016**, *33*, 2373–2387. [[CrossRef](#)] [[PubMed](#)]
15. Patra, J.; Das, G.; Fraceto, L.; Campos, E.; Rodriguez-Torres, M.; Acosta-Torres, L.; Diaz-Torres, L.; Grillo, R.; Swamy, M.; Sharma, S.; et al. Nano Based Drug Delivery Systems: Recent Developments and Future Prospects. *J. Nanobiotechnol.* **2018**, *16*, 1–33. [[CrossRef](#)]
16. Allen, M.; Tung, V.; Kaner, R. Honeycomb Carbon: A Review of Graphene. *Chem. Rev.* **2009**, *110*, 132–145. [[CrossRef](#)] [[PubMed](#)]
17. McCallion, C.; Burthem, J.; Rees-Unwin, K.; Golovanov, A.; Pluen, A. Graphene in Therapeutics Delivery: Problems, Solutions and Future Opportunities. *Eur. J. Pharm. Biopharm.* **2016**, *104*, 235–250. [[CrossRef](#)]
18. Yin, P.; Shah, S.; Chhowalla, M.; Lee, K. Design, Synthesis, and Characterization of Graphene–Nanoparticle Hybrid Materials for Bioapplications. *Chem. Rev.* **2015**, *115*, 2483–2531. [[CrossRef](#)]
19. Zhang, B.; Wang, Y.; Zhai, G. Biomedical Applications of The Graphene-Based Materials. *Mater. Sci. Eng. C* **2016**, *61*, 953–964. [[CrossRef](#)]

20. Patel, S.; Lee, S.; Lalwani, G.; Suhrland, C.; Chowdhury, S.; Sitharaman, B. Graphene-Based Platforms for Cancer Therapeutics. *Ther. Deliv.* **2016**, *7*, 101–116. [[CrossRef](#)]
21. Georgakilas, V.; Tiwari, J.; Kemp, K.; Perman, J.; Bourlinos, A.; Kim, K.; Zboril, R. Noncovalent Functionalization of Graphene and Graphene Oxide for Energy Materials, Biosensing, Catalytic, and Biomedical Applications. *Chem. Rev.* **2016**, *116*, 5464–5519. [[CrossRef](#)] [[PubMed](#)]
22. Liu, J.; Cui, L.; Losic, D. Graphene and Graphene Oxide as New Nanocarriers for Drug Delivery Applications. *Acta Biomater.* **2013**, *9*, 9243–9257. [[CrossRef](#)]
23. Shim, G.; Kim, M.; Park, J.; Oh, Y. Graphene-Based Nanosheets for Delivery of Chemotherapeutics and Biological Drugs. *Adv. Drug Deliv. Rev.* **2016**, *105*, 205–227. [[CrossRef](#)] [[PubMed](#)]
24. Bitounis, D.; Ali-Boucetta, H.; Hong, B.; Min, D.; Kostarelos, K. Prospects and Challenges of Graphene in Biomedical Applications. *Adv. Mater.* **2013**, *25*, 2258–2268. [[CrossRef](#)]
25. Yang, K.; Feng, L.; Liu, Z. Stimuli Responsive Drug Delivery Systems Based on Nano-Graphene for Cancer Therapy. *Adv. Drug Deliv. Rev.* **2016**, *105*, 228–241. [[CrossRef](#)]
26. Dembereldorj, U.; Kim, M.; Kim, S.; Ganbold, E.; Lee, S.; Joo, S. A Spatiotemporal Anticancer Drug Release Platform of Pegylated Graphene Oxide Triggered by Glutathione In Vitro and In Vivo. *J. Mater. Chem.* **2012**, *22*, 23845. [[CrossRef](#)]
27. Wen, H.; Dong, C.; Dong, H.; Shen, A.; Xia, W.; Cai, X.; Song, Y.; Li, X.; Li, Y.; Shi, D. Engineered Redox-Responsive PEG Detachment Mechanism in Pegylated Nano-Graphene Oxide for Intracellular Drug Delivery. *Small* **2012**, *8*, 760–769. [[CrossRef](#)] [[PubMed](#)]
28. Sahoo, N.; Bao, H.; Pan, Y.; Pal, M.; Kakran, M.; Cheng, H.; Li, L.; Tan, L. Functionalized Carbon Nanomaterials as Nanocarriers for Loading and Delivery of a Poorly Water-Soluble Anticancer Drug: A Comparative Study. *Chem. Commun.* **2011**, *47*, 5235. [[CrossRef](#)]
29. Angelopoulou, A.; Voulgari, E.; Diamanti, E.; Gournis, D.; Avgoustakis, K. Graphene Oxide Stabilized By PLA-PEG Copolymers for The Controlled Delivery of Paclitaxel. *Eur. J. Pharm. Biopharm.* **2015**, *93*, 18–26. [[CrossRef](#)] [[PubMed](#)]
30. Wang, C.; Li, J.; Amatore, C.; Chen, Y.; Jiang, H.; Wang, X. Gold Nanoclusters and Graphene Nanocomposites for Drug Delivery and Imaging of Cancer Cells. *Angew. Chem. Int. Ed.* **2011**, *50*, 11644–11648. [[CrossRef](#)] [[PubMed](#)]
31. Mo, R.; Jiang, T.; Sun, W.; Gu, Z. ATP-Responsive DNA-Graphene Hybrid Nanoaggregates for Anticancer Drug Delivery. *Biomaterials* **2015**, *50*, 67–74. [[CrossRef](#)]
32. Tian, J.; Luo, Y.; Huang, L.; Feng, Y.; Ju, H.; Yu, B. Pegylated Folate and Peptide-Decorated Graphene Oxide Nanovehicle for In Vivo Targeted Delivery of Anticancer Drugs and Therapeutic Self-Monitoring. *Biosens. Bioelectron.* **2016**, *80*, 519–524. [[CrossRef](#)]
33. Kim, H.; Lee, D.; Kim, J.; Kim, T.; Kim, W. Photothermally Triggered Cytosolic Drug Delivery Via Endosome Disruption Using a Functionalized Reduced Graphene Oxide. *ACS Nano* **2013**, *7*, 6735–6746. [[CrossRef](#)]
34. Zhang, W.; Guo, Z.; Huang, D.; Liu, Z.; Guo, X.; Zhong, H. Synergistic Effect of Chemo-Photothermal Therapy Using Pegylated Graphene Oxide. *Biomaterials* **2011**, *32*, 8555–8561. [[CrossRef](#)]
35. De, S.; Patra, K.; Ghosh, D.; Dutta, K.; Dey, A.; Sarkar, G.; Maiti, J.; Basu, A.; Rana, D.; Chattopadhyay, D. Tailoring the Efficacy of Multifunctional Biopolymeric Graphene Oxide Quantum Dot-Based Nanomaterial as Nanocargo in Cancer Therapeutic Application. *ACS Biomater. Sci. Eng.* **2018**, *4*, 514–531. [[CrossRef](#)] [[PubMed](#)]
36. Zhou, T.; Zhou, X.; Xing, D. Controlled Release of Doxorubicin from Graphene Oxide Based Charge-Reversal Nanocarrier. *Biomaterials* **2014**, *35*, 4185–4194. [[CrossRef](#)]
37. Yang, H.; Bremner, D.; Tao, L.; Li, H.; Hu, J.; Zhu, L. Carboxymethyl Chitosan-Mediated Synthesis of Hyaluronic Acid-Targeted Graphene Oxide for Cancer Drug Delivery. *Carbohydr. Polym.* **2016**, *135*, 72–78. [[CrossRef](#)] [[PubMed](#)]
38. Yang, X.; Wang, Y.; Huang, X.; Ma, Y.; Huang, Y.; Yang, R.; Duan, H.; Chen, Y. Multi-Functionalized Graphene Oxide Based Anticancer Drug-Carrier with Dual-Targeting Function and Ph-Sensitivity. *J. Mater. Chem.* **2011**, *21*, 3448–3454. [[CrossRef](#)]
39. Li, R.; Wang, Y.; Du, J.; Wang, X.; Duan, A.; Gao, R.; Liu, J.; Li, B. Graphene Oxide Loaded with Tumor-Targeted Peptide and Anti-Cancer Drugs for Cancer Target Therapy. *Sci. Rep.* **2021**, *11*, 1–10.
40. Zhang, L.; Xia, J.; Zhao, Q.; Liu, L.; Zhang, Z. Functional Graphene Oxide as A Nanocarrier for Controlled Loading and Targeted Delivery of Mixed Anticancer Drugs. *Small* **2010**, *6*, 537–544. [[CrossRef](#)]
41. Doxorubicin. Available online: <https://pubchem.ncbi.nlm.nih.gov/compound/doxorubicin> (accessed on 23 August 2021).
42. Al-malky, H.; Al Harthi, S.; Osman, A. Major Obstacles to Doxorubicin Therapy: Cardiotoxicity and Drug Resistance. *J. Oncol. Pharm. Pract.* **2019**, *26*, 434–444. [[CrossRef](#)] [[PubMed](#)]
43. Butowska, K.; Kozak, W.; Zdrowowicz, M.; Makurat, S.; Rychłowski, M.; Hać, A.; Herman-Antosiewicz, A.; Piosik, J.; Rak, J. Cytotoxicity of Doxorubicin Conjugated with C60 Fullerene. Structural and In Vitro Studies. *Struct. Chem.* **2019**, *30*, 2327–2338. [[CrossRef](#)]
44. Guo, Y.; Xu, H.; Li, Y.; Wu, F.; Li, Y.; Bao, Y.; Yan, X.; Huang, Z.; Xu, P. Hyaluronic Acid and Arg-Gly-Asp Peptide Modified Graphene Oxide with Dual Receptor-Targeting Function for Cancer Therapy. *J. Biomater. Appl.* **2017**, *32*, 54–65. [[CrossRef](#)] [[PubMed](#)]
45. Hossen, S.; Hossain, M.; Basher, M.; Mia, M.; Rahman, M.; Uddin, M. Smart Nanocarrier-Based Drug Delivery Systems for Cancer Therapy and Toxicity Studies: A Review. *J. Adv. Res.* **2019**, *15*, 1–18. [[CrossRef](#)] [[PubMed](#)]
46. Senapati, S.; Mahanta, A.; Kumar, S.; Maiti, P. Controlled Drug Delivery Vehicles for Cancer Treatment and Their Performance. *Signal. Transduct. Target. Ther.* **2018**, *3*, 1–19. [[CrossRef](#)]

47. Huda, S.; Alam, M.; Sharma, P. Smart Nanocarriers-Based Drug Delivery for Cancer Therapy: An Innovative and Developing Strategy. *J. Drug Deliv. Sci. Technol.* **2020**, *60*, 102018. [CrossRef]
48. Tang, Y.; Hu, H.; Zhang, M.; Song, J.; Nie, L.; Wang, S.; Niu, G.; Huang, P.; Lu, G.; Chen, X. An Aptamer-Targeting Photoresponsive Drug Delivery System Using “Off-On” Graphene Oxide Wrapped Mesoporous Silica Nanoparticles. *Nanoscale* **2015**, *7*, 6304–6310. [CrossRef]
49. Ma, X.; Tao, H.; Yang, K.; Feng, L.; Cheng, L.; Shi, X.; Li, Y.; Guo, L.; Liu, Z. A Functionalized Graphene Oxide-Iron Oxide Nanocomposite for Magnetically Targeted Drug Delivery, Photothermal Therapy, and Magnetic Resonance Imaging. *Nano Res.* **2012**, *5*, 199–212. [CrossRef]
50. Morgulchik, N.; Kamaly, N. Meta-Analysis of In Vitro Drug-Release Parameters Reveals Predictable and Robust Kinetics for Redox-Responsive Drug-Conjugated Therapeutic Nanogels. *ACS Appl. Nano Mater.* **2021**, *4*, 4256–4268. [CrossRef]
51. PubMed. Available online: <https://pubmed.ncbi.nlm.nih.gov/> (accessed on 13 August 2021).
52. Web of Science. Available online: <https://www.webofscience.com/wos/woscc/basic-search> (accessed on 13 August 2021).
53. Ovid: Welcome to Ovid. Available online: <https://ovidsp.ovid.com/> (accessed on 13 August 2021).
54. Digitize Graphs and Plots-Getdata Graph Digitizer-Graph Digitizing Software-Download. Available online: <http://getdata-graph-digitizer.com/download.php> (accessed on 15 August 2021).
55. Azadi, A.; Hamidi, M.; Rouini, M. Methotrexate-Loaded Chitosan Nanogels As ‘Trojan Horses’ for Drug Delivery to Brain: Preparation and In Vitro/In Vivo Characterization. *Int. J. Biol. Macromol.* **2013**, *62*, 523–530. [CrossRef]
56. Barzegar-Jalali, M. Kinetic Analysis of Drug Release from Nanoparticles. *J. Pharm. Pharm. Sci.* **2008**, *11*, 167. [CrossRef] [PubMed]
57. Azadi, S.; Ashrafi, H.; Azadi, A. Mathematical Modeling of Drug Release from Swellable Polymeric Nanoparticles. *J. Appl. Pharm. Sci.* **2017**, *7*, 125–133.
58. Pourtalebi Jahromi, L.; Ghazali, M.; Ashrafi, H.; Azadi, A. A Comparison of Models for The Analysis of the Kinetics of Drug Release from PLGA-Based Nanoparticles. *Heliyon* **2020**, *6*, e03451. [CrossRef] [PubMed]
59. Gouda, R.; Baishya, H.; Qing, Z. Application of Mathematical Models in Drug Release Kinetics of Carbidopa and Levodopa ER Tablets. *J. Dev. Drugs* **2017**, *6*, 1–8.
60. Bruschi, M. *Strategies to Modify the Drug Release from Pharmaceutical Systems*; Elsevier Science: Oxford, UK, 2015; pp. 63–86.
61. Standard Deviation of the Residuals: Sy.x, RMSE, RSDR-FAQ 1967-GraphPad. Available online: <https://www.graphpad.com/support/faq/standard-deviation-of-the-residuals-syx-rmse-rsdr/> (accessed on 13 August 2021).
62. GraphPad Software, L. GraphPad Prism 9 Curve Fitting Guide-Is the Slope Significantly Different Than Zero? Available online: [https://www.graphpad.com/guides/prism/latest/curve-fitting/istheslopesignificantlydifferentthanzero\\_.htm](https://www.graphpad.com/guides/prism/latest/curve-fitting/istheslopesignificantlydifferentthanzero_.htm) (accessed on 13 August 2021).
63. Prism-GraphPad. Available online: <https://www.graphpad.com/scientific-software/prism/> (accessed on 13 August 2021).
64. Zhang, Q.; Chi, H.; Tang, M.; Chen, J.; Li, G.; Liu, Y.; Liu, B. Mixed Surfactant Modified Graphene Oxide Nanocarriers for DOX Delivery to Cisplatin-Resistant Human Ovarian Carcinoma Cells. *RSC Adv.* **2016**, *6*, 87258–87269. [CrossRef]
65. Feng, L.; Li, K.; Shi, X.; Gao, M.; Liu, J.; Liu, Z. Smart Ph-Responsive Nanocarriers Based on Nano-Graphene Oxide for Combined Chemo- and Photothermal Therapy Overcoming Drug Resistance. *Adv. Healthc. Mater.* **2014**, *3*, 1261–1271. [CrossRef]
66. Han, C.; Zhang, C.; Ma, T.; Zhang, C.; Luo, J.; Xu, X.; Zhao, H.; Chen, Y.; Kong, L. Hypericin-Functionalized Graphene Oxide for Enhanced Mitochondria-Targeting and Synergistic Anticancer Effect. *Acta Biomater.* **2018**, *77*, 268–281. [CrossRef]
67. Karimi, S.; Namazi, H. Fe<sub>3</sub>O<sub>4</sub>@PEG-Coated Dendrimer Modified Graphene Oxide Nanocomposite as A Ph-Sensitive Drug Carrier for Targeted Delivery of Doxorubicin. *J. Alloys Compd.* **2021**, *879*, 160426. [CrossRef]
68. Alipour, N.; Namazi, H. Chelating Zno-Dopamine on The Surface of Graphene Oxide and Its Application as Ph-Responsive and Antibacterial Nanohybrid Delivery Agent for Doxorubicin. *Mater. Sci. Eng. C* **2020**, *108*, 110459. [CrossRef]
69. Ghamkhari, A.; Abbaspour-Ravasjani, S.; Talebi, M.; Hamishehkar, H.; Hamblin, M. Development of A Graphene Oxide-Poly Lactide Nanocomposite as A Smart Drug Delivery System. *Int. J. Biol. Macromol.* **2021**, *169*, 521–531. [CrossRef]
70. Ma, N.; Liu, J.; He, W.; Li, Z.; Luan, Y.; Song, Y.; Garg, S. Folic Acid-Grafted Bovine Serum Albumin Decorated Graphene Oxide: An Efficient Drug Carrier for Targeted Cancer Therapy. *J. Colloid Interface Sci.* **2017**, *490*, 598–607. [CrossRef]
71. Jin, R.; Ji, X.; Yang, Y.; Wang, H.; Cao, A. Self-Assembled Graphene-Dextran Nanohybrid for Killing Drug-Resistant Cancer Cells. *ACS Appl. Mater. Interfaces* **2013**, *5*, 7181–7189. [CrossRef]
72. Yang, X.; Zhang, X.; Liu, Z.; Ma, Y.; Huang, Y.; Chen, Y. High-Efficiency Loading and Controlled Release of Doxorubicin Hydrochloride on Graphene Oxide. *J. Phys. Chem. C* **2008**, *112*, 17554–17558. [CrossRef]
73. Li, S.; Xiao, L.; Deng, H.; Shi, X.; Cao, Q. Remote Controlled Drug Release from Multi-Functional Fe<sub>3</sub>O<sub>4</sub>/GO/Chitosan Microspheres Fabricated by An Electrospray Method. *Colloids Surf. B Biointerfaces* **2017**, *151*, 354–362. [CrossRef]
74. Hu, H.; Yu, J.; Li, Y.; Zhao, J.; Dong, H. Engineering of A Novel Pluronic F127/Graphene Nanohybrid for Ph Responsive Drug Delivery. *J. Biomed. Mater. Res. Part A* **2011**, *100*, 141–148. [CrossRef]
75. Hashemi, H.; Namazi, H. Sonochemically Synthesized Blue Fluorescent Functionalized Graphene Oxide as A Drug Delivery System. *Ultrason. Sonochem.* **2018**, *42*, 124–133. [CrossRef]
76. Samadian, H.; Mohammad-Rezaei, R.; Jahanban-Esfahlan, R.; Massoumi, B.; Abbasian, M.; Jafarizad, A.; Jaymand, M. A De Novo Theranostic Nanomedicine Composed of Pegylated Graphene Oxide and Gold Nanoparticles for Cancer Therapy. *J. Mater. Res.* **2020**, *35*, 430–441. [CrossRef]

77. Wu, J.; Wang, Y.; Yang, X.; Liu, Y.; Yang, J.; Yang, R.; Zhang, N. Graphene Oxide Used as A Carrier for Adriamycin Can Reverse Drug Resistance in Breast Cancer Cells. *Nanotechnology* **2012**, *23*, 355101. [CrossRef] [PubMed]
78. Shi, J.; Wang, L.; Zhang, J.; Ma, R.; Gao, J.; Liu, Y.; Zhang, C.; Zhang, Z. A Tumor-Targeting Near-Infrared Laser-Triggered Drug Delivery System Based On GO@Ag Nanoparticles for Chemo-Photothermal Therapy and X-Ray Imaging. *Biomaterials* **2014**, *35*, 5847–5861. [CrossRef]
79. Mauro, N.; Scialabba, C.; Agnello, S.; Cavallaro, G.; Giammona, G. Folic Acid-Functionalized Graphene Oxide Nanosheets Via Plasma Etching as A Platform to Combine NIR Anticancer Phototherapy and Targeted Drug Delivery. *Mater. Sci. Eng. C* **2020**, *107*, 110201. [CrossRef]
80. Guo, S.; Huang, L. Nanoparticles Escaping RES and Endosome: Challenges for Sirna Delivery for Cancer Therapy. *J. Nanomater.* **2011**, *2011*, 1–12. [CrossRef]
81. Georgieva, M.; Gospodinova, Z.; Keremidarska-Markova, M.; Kamenska, T.; Gencheva, G.; Krasteva, N. Pegylated Nanographene Oxide in Combination with Near-Infrared Laser Irradiation as A Smart Nanocarrier in Colon Cancer Targeted Therapy. *Pharmaceutics* **2021**, *13*, 424. [CrossRef] [PubMed]
82. Suk, J.; Xu, Q.; Kim, N.; Hanes, J.; Ensign, L. Pegylation as A Strategy for Improving Nanoparticle-Based Drug and Gene Delivery. *Adv. Drug Deliv. Rev.* **2016**, *99*, 28–51. [CrossRef]
83. Shen, S.; Wu, Y.; Liu, Y.; Wu, D. High Drug-Loading Nanomedicines: Progress, Current Status, and Prospects. *Int. J. Nanomed.* **2017**, *12*, 4085–4109. [CrossRef]
84. Diaz-Diestra, D.; Thapa, B.; Badillo-Diaz, D.; Beltran-Huarac, J.; Morell, G.; Weiner, B. Graphene Oxide/Zns:Mn Nanocomposite Functionalized with Folic Acid As A Nontoxic and Effective Theranostic Platform for Breast Cancer Treatment. *Nanomaterials* **2018**, *8*, 484. [CrossRef] [PubMed]
85. Nys, G.; Fillet, M. Microfluidics Contribution to Pharmaceutical Sciences: From Drug Discovery to Post Marketing Product Management. *J. Pharm. Biomed. Anal.* **2018**, *159*, 348–362. [CrossRef]
86. Wang, Z.; Colombi Ciacchi, L.; Wei, G. Recent Advances in The Synthesis of Graphene-Based Nanomaterials for Controlled Drug Delivery. *Appl. Sci.* **2017**, *7*, 1175. [CrossRef]
87. Hoseini-Ghahfarokhi, M.; Mirkiani, S.; Mozaffari, N.; Abdolahi Sadatlu, M.; Ghasemi, A.; Abbaspour, S.; Akbarian, M.; Farjadain, F.; Karimi, M. Applications of Graphene and Graphene Oxide in Smart Drug/Gene Delivery: Is the World Still Flat? *Int. J. Nanomed.* **2020**, *15*, 9469–9496. [CrossRef]
88. Amina, S.; Guo, B. A Review on The Synthesis and Functionalization of Gold Nanoparticles as A Drug Delivery Vehicle. *Int. J. Nanomed.* **2020**, *15*, 9823–9857. [CrossRef]
89. Peppas, N.; Narasimhan, B. Mathematical Models in Drug Delivery: How Modeling Has Shaped the Way We Design New Drug Delivery Systems. *J. Control. Release* **2014**, *190*, 75–81. [CrossRef]
90. Mircioiu, C.; Voicu, V.; Anuta, V.; Tudose, A.; Celia, C.; Paolino, D.; Fresta, M.; Sandulovici, R.; Mircioiu, I. Mathematical Modeling of Release Kinetics from Supramolecular Drug Delivery Systems. *Pharmaceutics* **2019**, *11*, 140. [CrossRef] [PubMed]
91. Costa, P.; Sousa Lobo, J. Modeling and Comparison of Dissolution Profiles. *Eur. J. Pharm. Sci.* **2001**, *13*, 123–133. [CrossRef]
92. Dash, S.; Murthy, P.; Nath, L.; Chowdhury, P. Kinetic Modeling on Drug Release from Controlled Drug Delivery Systems. *Acta Pol. Pharm.* **2010**, *67*, 217–223. [PubMed]
93. Siepmann, J.; Peppas, N. Modeling of Drug Release from Delivery Systems Based on Hydroxypropyl Methylcellulose (HPMC). *Adv. Drug Deliv. Rev.* **2012**, *64*, 163–174. [CrossRef]
94. Chang, Y.; Yang, S.; Liu, J.; Dong, E.; Wang, Y.; Cao, A.; Liu, Y.; Wang, H. In Vitro Toxicity Evaluation of Graphene Oxide on A549 Cells. *Toxicol. Lett.* **2011**, *200*, 201–210. [CrossRef] [PubMed]
95. Foroozandeh, P.; Aziz, A. Insight into Cellular Uptake and Intracellular Trafficking of Nanoparticles. *Nanoscale Res. Lett.* **2018**, *13*. [CrossRef] [PubMed]
96. Kaźmierczak, Z.; Szostak-Paluch, K.; Przybyło, M.; Langner, M.; Witkiewicz, W.; Jędruchniewicz, N.; Dąbrowska, K. Endocytosis in Cellular Uptake of Drug Delivery Vectors: Molecular Aspects in Drug Development. *Bioorg. Med. Chem.* **2020**, *28*, 115556. [CrossRef] [PubMed]
97. Hua, S.; de Matos, M.; Metselaar, J.; Storm, G. Current Trends and Challenges in The Clinical Translation of Nanoparticulate Nanomedicines: Pathways for Translational Development and Commercialization. *Front. Pharmacol.* **2018**, *9*, 790. [CrossRef]
98. Douedi, S.; Carson, M.P. *Anthracycline Medications (Doxorubicin) StatPearls*; StatPearls Publishing: Treasure Island, FL, USA, 2021.
99. Doxorubicin Dosage Guide + Max Dose, Adjustments—Drugs.com. Available online: [https://www.drugs.com/dosage/doxorubicin.html#Usual\\_Adult\\_Dose\\_for\\_Breast\\_Cancer](https://www.drugs.com/dosage/doxorubicin.html#Usual_Adult_Dose_for_Breast_Cancer) (accessed on 28 August 2021).
100. Eksborg, S. Pharmacokinetics of Anthracyclines. *Acta Oncol.* **1989**, *28*, 873–876. [CrossRef] [PubMed]
101. Lipinski, C.; Lombardo, F.; Dominy, B.; Feeney, P. Experimental and Computational Approaches to Estimate Solubility and Permeability in Drug Discovery and Development. *Adv. Drug Deliv. Rev.* **2001**, *46*, 3–26. [CrossRef]